

# Method to Quantify the Black Carbon Aerosol Light Absorption Enhancement with Mixing State Index

Gang Zhao<sup>1</sup>, Tianyi Tan<sup>1</sup>, Yishu Zhu<sup>1</sup>, Min Hu<sup>1</sup>, Chunsheng Zhao<sup>2\*</sup>

<sup>1</sup> State Key Joint Laboratory of Environmental Simulation and Pollution Control, International Joint Laboratory for Regional Pollution Control, Ministry of Education, College of Environmental Sciences and Engineering, Peking University, Beijing, 100871, China

<sup>2</sup> Department of Atmospheric and Oceanic Sciences, School of Physics, Peking University, Beijing, 100871, China

\*Correspondence author: Chunsheng Zhao (zcs@pku.edu.cn)

## Abstract

Large uncertainties remain when estimating the warming effects of ambient black carbon (BC) aerosols on climate. One of the key challenges in modeling the radiative effects is predicting the BC light absorption enhancement, which is mainly determined by the mass ratio of non-BC coating material to BC in the population of BC-containing aerosols (MR). For the same MR, recent researches find that the radiative absorption enhancements by BC are also controlled by its particle-to-particle heterogeneity. In this study, the BC mixing state index ( $\chi$ ) is developed to quantify the dispersion of ambient black carbon aerosol mixing states based on binary systems of BC and other non-black carbon components. We demonstrate that the BC light absorption enhancement increases with  $\chi$  for the same MR, which indicates that  $\chi$  can be employed as a factor to constrain the light absorption enhancement of ambient BC. Our framework can be further used in the model to study the black carbon radiative effects on climate change.

## 1 Introduction

Black carbon (BC) aerosols absorb solar radiation, thus exert warming effects on the earth's energy system (Bond and Bergstrom, 2006; Bond et al., 2013). However, large uncertainties remain when quantifying the BC warming effects (Cui et al., 2016; Jacobson, 2010; Koch et al., 2009; Menon et al., 2002). Most of the BC particles were emitted from incomplete combustion of bio-fossil fuel

28 (Bond et al., 2013). After initially emitted, the BC particles would experience aging processing with  
29 some other non-BC components coated on the BC particles (Peng et al., 2017;Peng et al., 2016).  
30 During the aging processing, the light absorption of BC aerosols would increase, which is well  
31 known as “lensing effect” (Saleh et al., 2013;Saleh et al., 2014). One critical challenge in estimating  
32 the BC warming effects is quantifying the “lensing effects” of ambient BC aerosols (Liu et al., 2017).

33 The light absorption enhancement ( $E_{abs}$ ), which is the ratio of light absorption of BC aerosols  
34 with the coating to that of bare BC particles, is proposed to quantify the “lensing effects”.  
35 Comprehensive studies have been carried out to study the  $E_{abs}$  (Liu et al., 2017;Peng et al.,  
36 2016;Liu et al., 2015;Fierce et al., 2016;Fierce et al., 2020;Cappa et al., 2012). However, a large  
37 discrepancy remains between the results of  $E_{abs}$  from field measurements and laboratory studies.  
38 The measured  $E_{abs}$  of laboratory generated monodisperse BC particles can reach up to a factor of 2,  
39 which is consistent with the results from the Mie scattering model (Cappa et al., 2012;Cappa et al.,  
40 2019). However, some field measurement shows that the  $E_{abs}$  of ambient BC aerosols are relatively  
41 small, with 1.06 at California (Cappa et al., 2012), 1.07 in South China (Lan et al., 2013), and 1.10 in  
42 Japan (Nakayama et al., 2014), while the measured  $E_{abs}$  of ambient BC reaches 1.59 during  
43 summer time in Beijing (Xie et al., 2019).

44 Many factors, such as the morphology of the BC core, the position of BC core inside coating, the  
45 coating thickness, chemical properties of coating materials, and size distribution of the BC, would  
46 influence the  $E_{abs}$  of ambient BC aerosols. Wu et al. (2018) reported that the BC light absorption  
47 properties vary significantly for different morphology from the calculation of models. Laboratory  
48 studies also find that the light absorption properties of the BC core were tuned due to the change of  
49 the BC core morphology (Yuan et al., 2020). Comparing with the concentric spherical structure, the  
50 off-center coated BC aggregates would lead to up to a 31% reduction in  $E_{abs}$  by the multiple-sphere  
51 T-matrix method (Zhang et al., 2017). It has been well studied that the  $E_{abs}$  is highly related with  
52 the mass ratio of coating materials and BC core (MR) (Liu et al., 2014;Liu et al., 2017). The coating  
53 material are also critical in regulating the morphology and optical properties as the coating of sulfuric  
54 acid has been shown to be more efficient in altering the BC morphology and light absorption(Zhang

55 et al., 2008;Xue et al., 2009b, a). Zhao et al. (2019b) reported that the light absorption properties of  
56 ambient BC particles are influenced by BC mass size distribution. Besides, recently researchers  
57 found that the  $E_{abs}$  are also controlled by particle-to-particle heterogeneity (Fierce et al.,  
58 2016;Fierce et al., 2020). As shown in Fig.1, the  $E_{abs}$  of ambient aerosols for the same MR would  
59 vary by about 30%, which is consistency with the results of Fierce et al. (2020). However, there is no  
60 study, to our best knowledge, that constrains the uncertainties of the  $E_{abs}$  for the same MR.

61 In this study, we developed a BC mixing states index ( $\chi$ ) to quantify the dispersion of black  
62 carbon aerosol mixing states based on binary systems of BC and other non-black carbon components.  
63 We demonstrate that the BC  $E_{abs}$  increases with  $\chi$  for the same MR based on the field measurement,  
64 which indicates that  $\chi$  can be employed as a factor to constrain the  $E_{abs}$  properties of ambient BC.

## 65 **2 Data and methods**

### 66 **2.1 Field measurement**

67 The field measurements were conducted at a suburban site Taizhou (119°57' E, 32°35' N) from  
68 26 May to 18 June. As shown in Fig. S1, the Taizhou site lies between two large cities of Nanjing  
69 and Shanghai, where the aerosols can be seen as representative that of the Yangtze River Delta area  
70 (Liu et al., 2020). More details of the field measurements can refer to Zhao et al. (2019a). During the  
71 field measurement, we placed all of the instruments in a container where the temperature was  
72 carefully controlled between 22 and 26 °C. A PM<sub>10</sub> impactor, which is about 5 meters above the  
73 ground, was mounted on the top of the container. The sample aerosols were drawn from the impactor  
74 and then dried by a Nafion dryer tube.

75 The size-resolved BC core distribution and non-BC coating thickness were measured by using a  
76 differential mobility analyzer (DMA, model 3081, TSI, USA) in tandem with a single-particle soot  
77 photometer (SP2, Droplet Measurement Technologies, USA). Detailed information on the DMA can  
78 refer to Zhao et al. (2019c). SP2 can measure the BC mass concentration from the incandescence  
79 signals emitted by the BC particle, which is heated to around 6000 K by laser with a wavelength of  
80 1064 nm (Zhao et al., 2020b). Along with the measurement of size-resolved BC distributions, a

81 nephelometer (Aurora 300, Ecotech, Australia) (Müller et al., 2011) was employed to measure the  
82 aerosol scattering coefficient ( $\sigma_{sca}$ ) at the wavelength of 525 nm.

## 83 **2.2 BC mixing states from DMA-SP2 system**

84 In this study, the SP2 was placed after the DMA to measure the size-selected distribution of  
85 BC-core and non-BC coating thickness. The schematic instrument setup is shown in Fig. S1 and the  
86 details can refer to part 1 in the supplementary material. After careful calibrations of the SP2 (part  
87 2.1 in the supplementary material), transformations of the measured signals to BC mass  
88 concentrations (part 2.2 in the supplementary material), and multiple charging corrections (part 2.3 in  
89 the supplementary material), the BC-containing number concentration distribution under different  
90 total diameter ( $D_p$ ) and BC core diameter ( $D_c$ ) can be calculated, as shown in Fig. S4 (b). The details  
91 of the calculation of size-resolved distribution of BC core and coating thickness from the DMA-SP2  
92 system can refer to Zhao et al. (2020a). The measured size-resolved distribution of BC core and  
93 coating thickness as in Fig. S4(b) were used for further analysis. It should be mentioned that the  
94 measured number distribution of BC-containing aerosols is two dimensional ( $\frac{d^2N}{d\log D_p \cdot d\log D_c}$ ). As noted  
95 by Zhao et al. (2020b), the SP2 can only detect these BC-containing aerosols with core diameter  
96 larger than 84 nm. The DMA select the aerosol at the range between 13.3 nm and 749.9 nm. In the  
97 following discussion, the size-resolved distribution of BC core and coating thickness are constrained  
98 in the range between 84 and 749.9 nm.

## 99 **2.3 Calculating the aerosol optical properties**

### 100 **2.3.1 Calculating the aerosol absorption coefficient for a given $D_p$ and $D_c$**

101 A Mie scattering model (Bohren and Huffman, 2007) was employed to calculate the aerosol  
102 absorption coefficient ( $\sigma_{abs}$ ). When calculating the  $\sigma_{abs}$  of single particle, the Mie scattering model  
103 requires the diameter of the core, the coating thickness, the refractive index of the core, and the  
104 refractive index of the shell. The refractive index of the core adopted here is  $1.67+0.67i$ , which is the  
105 calculated mean value by comparing the measured light absorption and calculated light absorption  
106 properties (Zhao et al., 2020a). The refractive index of the shell is chosen to be  $1.46+0i$ , which is  
107 assumed to be as that of the non-BC component measured by the DMA-SP2 system (Zhao et al.,

108 2019a;Zhao et al., 2019c). With the above information, the  $\sigma_{abs}$  values at a given  $D_p$  and a given  $D_c$   
109 can be calculated.

### 110 2.3.2 Calculating the aerosol bulk absorption coefficient

111 We calculate the single-particle  $\sigma_{abs}$  of different  $D_p$  and  $D_c$  with the given refractive index of  
112 core and shell and then the ambient aerosol  $\sigma_{abs}$  distributions at different  $D_p$  and  $D_c$  ( $\frac{d^2\sigma_{abs}}{d\log D_p \cdot d\log D_c}$ )  
113 can be calculated by multiplying the number concentrations of the BC-contained aerosols  
114 ( $\frac{d^2N}{d\log D_p \cdot d\log D_c}$ ). By integrating the  $\frac{d^2\sigma_{abs}}{d\log D_p \cdot d\log D_c}$  over different  $D_c$  values, the ambient aerosol  $\sigma_{abs}$   
115 distribution along with different  $D_p$  ( $\frac{d\sigma_{abs}}{d\log D_p}$ ) can be calculated. The total  $\sigma_{abs}$  of the ambient  
116 BC-containing aerosols can be calculated by integrating the  $\frac{d\sigma_{abs}}{d\log D_p}$  over different  $D_p$  values.

### 117 2.3.3 Calculating the aerosol $E_{abs}$

118 Along with calculating the  $\sigma_{abs}(D_p, D_c)$  of single-particle for different  $D_p$  and  $D_c$ , we calculate  
119 the corresponding light absorption ( $\sigma_{abs}(D_c, D_c)$ ) value for  $D_c$  without thickness. The corresponding  
120 total light absorption of all measured BC-contained aerosols without coating can be calculated by  
121 integrating the calculated  $\sigma_{abs}(D_c, D_c)$  among different  $D_p$  and  $D_c$  weighted with  $\frac{d^2N}{d\log D_p \cdot d\log D_c}$ . Thus  
122 the ambient BC particles without coating ( $\sigma_{abs}(D_p = D_c)$ ) can be calculated. The bulk ambient  
123 aerosol  $E_{abs}$  can thus be calculated with  $E_{abs} = \frac{\sigma_{abs}}{\sigma_{abs}(D_p = D_c)}$ .

### 124 2.4 Quantifying BC mixing states

125 In this study, the mass-weighted mixing state index for BC-containing particles ( $\chi$ ) is developed  
126 to investigate the distribution of non-BC material across the BC-containing particle population,  
127 which is essentially the same as that of Yu et al. (2020). As for BC particles with known  $D_p$  and  $D_c$ ,  
128 the mass concentration of BC core and coating material can be calculated with the effective density  
129 of BC core and coating material. The effective density of the BC core is calculated in detail in  
130 section 2.2 in the supplement. The effective density of the coating material is assumed to be the same  
131 as the measured effective density of non-BC aerosols by using a centrifugal particle mass analyzer  
132 (version 1.53, Cambustion Ltd, UK) in tandem with a scanning mobility particle sizer system (Zhao  
133 et al., 2019a) and a mean value of 1.5 g/cm<sup>3</sup> was used here.

134 For each of the particle  $i$  ( $i=1,2,\dots, N$  is the measured BC-containing aerosol number  
 135 concentration), we can calculate its mass ratio of BC with

$$136 \quad p_{i,BC} = \frac{m_{i,BC}}{m_i}, \quad (1)$$

137 where  $m_{i,BC}$  is the mass concentration of BC and  $m_i$  is the total mass concentration of particle  $i$ .  
 138 The mass portion of BC can be calculated as

$$139 \quad p_{BC} = \frac{m_{BC}}{m_{tot}}, \quad (2)$$

140 where  $m_{BC}$  (the total mass concentration of BC) and  $m_{tot}$  (total mass of BC-containing aerosols)  
 141 can be calculated as  $m_{BC} = \sum_{i=1}^N m_{i,BC}$ ,  $m_{tot} = \sum_{i=1}^N m_i$ . The MR is calculated as:

$$142 \quad MR = \frac{(m_{tot}-m_{BC})}{m_{BC}}, \quad (3)$$

143 The mass portion of particle  $i$  to total BC-containing aerosols is calculated as

$$144 \quad p_i = \frac{m_i}{m_{tot}}. \quad (4)$$

145 With the definition above, we can calculate the mixing entropy of particle  $i$  ( $H_i$ ) by:

$$146 \quad H_i = - (p_{i,BC} \ln(p_{i,BC}) + (1 - p_{i,BC}) \ln(1 - p_{i,BC})), \quad (5)$$

147 the average mixing entropy of the population by:

$$148 \quad H_\alpha = \sum_{i=1}^N p_i H_i, \quad (6)$$

149 And the population bulk mixing entropy by:

$$150 \quad H_\gamma = - (p_{BC} \ln(p_{BC}) + (1 - p_{BC}) \ln(1 - p_{BC})). \quad (7)$$

151 Then the average particle species diversity can be calculated by

$$152 \quad D_\alpha = e^{H_\alpha}, \quad (8)$$

153 And the bulk population species diversity can be calculated by

$$154 \quad D_\gamma = e^{H_\gamma}, \quad (9)$$

155 With the above information, the dispersion of BC particle mixing states can be defined as:

$$156 \quad \chi = \frac{D_\alpha - 1}{D_\gamma - 1}. \quad (10)$$

157 The basic idea of quantifying the BC particle mixing states is the same as that of Riemer and  
 158 West (2013) and Riemer et al. (2019), their framework mainly focuses on the bulk ambient aerosols

159 with about five species (Bondy et al., 2018;Ye et al., 2018). A number of different (binary) species  
160 definitions for  $\chi$  have been used in the literature. Ching et al. (2017) used this index to study the  
161 impact of mixing of hygroscopic and non-hygroscopic species on cloud condensation nuclei. Dickau  
162 et al. (2016) quantified the volatile and nonvolatile species mixing characters. Zheng et al. (2021)  
163 compared three different variants for  $\chi$ , one of which was based on absorbing (BC) and  
164 non-absorbing species, and Yu et al. (2020) use a metric which is very related to this paper. Our  
165 developed  $\chi$  is a reduced parameter that only concerns the BC-containing aerosols with two species  
166 of BC component and non-BC coating materials.

### 167 **3. Results and Discussions**

#### 168 **3.1 BC mixing states diagram**

169 A mixing state diagram as shown in Fig. 2 was employed for better understanding the dispersion  
170 of BC mixing states. Nine different aerosols populations were given and summarized in Table 1. For  
171 each group, we include six BC-containing particles with different mass concentrations of BC core  
172 and non-BC coating material.

173 For group 1, the amounts of BC are very small (near zero) and most of the aerosols are  
174 composed of the non-BC component. The  $D_\alpha$  and  $D_\gamma$  values are 1.00 and 1.00 respectively. These  
175 groups can also be described as all of the particles are pure BC particles without coating.

176 For groups 2, 3, and 4, the mass concentration ratios of the BC component to the non-BC  
177 component are 1:5, 2:4, and 3:3 respectively. All of the  $D_\alpha$  values are 1.00 for groups 2, 3, and 4  
178 because the BC particles are externally mixed. The corresponding  $D_\gamma$  values are 1.56, 1.89, and  
179 2.00 respectively. For these three groups, the  $\chi$  values are all 0.00.

180 For groups 4, 5, 6, and 7, the mass concentration ratios of the BC component to the non-BC  
181 component are all 1:1 while the BC component is mixed to a different extent. It is easy to conclude  
182 that the BC particles of group 7 are most well mixed among these four groups. The corresponding  $\chi$   
183 values are 0, 0.26, 0.83, and 1.0 for group 4, 5, 6, and 7, respectively.

184 As for groups 8 and 9, the mass concentration ratios of the BC component to the non-BC  
185 component are 1:6.1. The  $D_\gamma$  values are 1.5 and the  $D_\alpha$  values are 1.5 and 1.35 respectively.

186 From the different group, the average particle species diversity  $D_\gamma$  value is mainly determined  
187 by the total mass concentration ratio of the BC component to the non-BC component. It varies  
188 between 1 and 2 for different total mass concentration ratios. The  $D_\gamma$  increases when the mass ratio  
189 approaches 1. The bulk population species diversity  $D_\alpha$  ranges between 1 and  $D_\gamma$ . It denotes the  
190 diversity of different BC-containing particles.

### 191 3.2 Overview of the measurement

192 Fig.S6 gives the time series of our field measurements results. During the field measurement, the  
193  $\sigma_{sca}$  varies between 29 and 1590  $\text{Mm}^{-1}$ . The ranges of  $H_\alpha$ ,  $H_\gamma$ ,  $D_\alpha$ ,  $D_\gamma$ , and  $\chi$  are 0.10~0.55,  
194 0.42~0.64, 1.32~1.72, 1.52~1.91 and 0.62~0.82 respectively.

195 For a better understanding of the characteristics of the above parameters, we only present the  
196 time series of these parameters during a pollution period between 27, May and 30, May in Fig. 3. As  
197 shown in Fig. 3, the MR increased from about 2 to 4 when the  $\sigma_{sca}$  increased from 300 to 1200  
198  $\text{Mm}^{-1}$ , which indicates that some secondary aerosol components were coated on the BC particles  
199 when the ambient air is more polluted. During the aging processing, the  $H_\alpha$  decreased from 0.51 to  
200 0.38 and  $H_\gamma$  decreased from 0.63 to 0.49. The  $D_\alpha$  decreases from 1.66 to 1.48. The  $D_\gamma$  decreases  
201 with the MR from 1.86 to 1.66, which is consistent with the results in section 3.1 that the  $D_\gamma$  should  
202 decrease with the MR when the MR is larger than 1. The  $\chi$  varies between 0.68 and 0.79. It is worth  
203 noting that the  $\chi$  is not well correlated with the pollution conditions.

204 The daily variation of  $\sigma_{sca}$ , which is highly related to the development of the boundary layer,  
205 reaches its maximum value of 525  $\text{Mm}^{-1}$  at 6:00 AM and a minimum value of 150  $\text{Mm}^{-1}$  at 7:00 PM.  
206 The daily variation of MR is largest at 5:00 AM with a mean value of 3.16 and reaches its minimum  
207 value of 2.56 at 7:00 PM. The daily variation of MR was mainly influenced by aging processing and  
208 anthropogenic activities. During the daytime, the newly emitted BC particles due to anthropogenic  
209 activities have low MR and the measured mean MR is low than that at night. The  $D_\alpha$  values, which  
210 are anti-correlated with MR, show the opposite trend with MR. As for  $\chi$ , it is smaller in the daytime  
211 than that at night. The lower  $\chi$  values at daytime mainly resulted from the mixing of newly emitted  
212 BC particles due to anthropogenic activities and some pre-existed aged BC particles.



### 213 **3.3 Relationship between the $\chi$ and $E_{abs}$ from measurement**

214 For each of the measured group of size-resolved distribution of BC core and coating thickness, we  
215 calculated the corresponding MR,  $\chi$ , and  $E_{abs}$ . And the relationship between the MR and absorption  
216 enhancement is summarized in Fig. 5. It should be noted that the shown BC population is only one of  
217 possible examples with  $\chi$  equaling 0, 0.81, and 1 respectively. There are many other possible ways  
218 the particle composition can be arranged that would give the same mixing state index.

219 Overall, the BC  $E_{abs}$  increase with MR, which is consistent with the previous knowledge. For a  
220 given value of MR,  $E_{abs}$  varies by about 20%, especially for these conditions with MR larger than  
221 1.0. When MR is larger than 1.0, the  $E_{abs}$  increase with the  $\chi$ . Relationship between the  $E_{abs}$  and  $\chi$   
222 is rather complex when MR is smaller than 1.0. However, only 448 of 6948 groups (6.4%) of the  
223 measured MR values are smaller than 1. Therefore, for most of the conditions, the measured  $E_{abs}$   
224 should increase with  $\chi$ , which indicates that the BC mixing state index  $\chi$  can be employed as a factor  
225 to constrain the  $E_{abs}$  of ambient aerosols.

226 A schematic diagram as shown in Fig. 6 to denotes the relationship between the  $E_{abs}$  and  $\chi$ .  
227 From Fig. 6, we calculated the  $E_{abs}$  and  $\chi$  under differ MR and then compared the  $E_{abs}$  of different  
228 bulk aerosols. The first group contains two particles with both the MR equaling 8. The corresponding  
229  $\chi$  is 1.00 and  $E_{abs}$  is 1.60. Another group of particles contains two particles with MR equaling 1 and  
230 15, respectively. Thus the second group of particles has a mean MR of 8. The calculated  
231 corresponding  $\chi$  and  $E_{abs}$  are 0.79 and 1.42 respectively. Thus, the  $E_{abs}$  tend to increase with  $\chi$  for  
232 the same MR, which is mainly resulted from that the increasing ratio of  $E_{abs}$  (the slope of  $E_{abs}$  to  
233 MR) decrease with MR.

234 It is worth noting that the increasing ratio is almost the same when the MR is in the range of 0  
235 and 3. Therefore, the  $E_{abs}$  doesn't tend to increase with the  $\chi$  when the MR was less than 1, which  
236 is consistent with our study as shown in Fig. 6.

### 237 **3.4 Relationship between the $\chi$ and $E_{abs}$ from simulation**

238 A Mont-Carlo simulation was carried out for a better understanding of the relationship between  
239  $\chi$  and  $E_{abs}$ . During the simulation, the number of BC-containing particles was assumed to be 30. For  
240 each of the BC particle, the core diameter of the BC particle was randomly generated with a

241 geometric mean diameter of 130.7 nm and a geometric standard deviation of 1.5, which is the mean  
242 measurement results of the BC core distribution during the field measurement (Zhao et al., 2020b).  
243 The corresponding MR of the BC particle is assumed to be in the range between 0.0 (pure BC  
244 particles without coating) and 78.0 (particles with a core diameter of 130 nm and a total diameter of  
245 560 nm). For each of the group of particles, the corresponding aerosol bulk MR,  $E_{abs}$  and  $\chi$  can be  
246 calculated. The simulations were conducted for  $10^7$  times, and the calculated mean and standard  
247 deviation of  $E_{abs}$  under different MR and  $\chi$  are summarized in Fig. 7 (a) and (b).

248 From Fig. 7 (a), the calculated  $E_{abs}$  tend to increase with MR for each of the given  $\chi$ , which is  
249 consistent with the previous knowledge of the BC light absorption properties. Then the MR is  
250 smaller than 2, the calculated  $E_{abs}$  does not seem to increase with the  $\chi$ , which is consistent with the  
251 analyzed results from section 3.3 and Fig. 6. When the MR is larger 2, the  $E_{abs}$  tend to increase  
252 with the  $\chi$ . The larger the MR is, the  $E_{abs}$  is more sensitive to  $\chi$ . Two reasons may lead to this  
253 phenomenon. One reason is that that calculated slope of  $E_{abs}$  to MR for one particle as shown in Fig.  
254 6 decreases with the MR. Another reason is that the calculated  $E_{abs}$  range increase with MR when  
255 the  $\chi$  changes between 0 and 1 as shown in Fig. 5.

256 As for the uncertainties of simulated  $E_{abs}$ , it tends to increase with the MR, which is consistent  
257 with the previous discussions that the  $E_{abs}$  the range tends to increase with MR. Overall, the  
258 calculated standard deviations of  $E_{abs}$  are all the way smaller than 10% for different MR and  $\chi$ .  
259 Therefore, the calculated  $E_{abs}$  can be well constrained by  $\chi$ .

#### 260 **4 Conclusion**

261 Larger uncertainties remain when estimating the warming effects of ambient BC aerosols due to  
262 the poor understanding of the ambient BC light absorption enhance ratio. Previous studies find that  
263 the light absorption of ambient aerosols was mainly determined by the morphology of the BC core,  
264 the position of the BC core inside coating, the coating thickness, and the size distribution of the BC.  
265 We find that there are more than 20% of uncertainties for the same measured mean coating thickness,  
266 i.e. the same measured MR based on the field measurement of the size-resolved distribution of BC

267 core and coating thickness. However, there were no-study, to our best knowledge, that attempts to  
268 constrain the uncertainties.

269 In this study, we developed the BC mixing states index  $\chi$  based on the mass concentrations of  
270 BC components and non-BC material of each BC-containing particle. Results show that the light  
271 absorption enhancement ratio  $E_{abs}$  tend to increase the  $\chi$  for the same measured MR. Therefore, our  
272 developed parameter  $\chi$ , which reflects the dispersion of the BC mixing states, can be employed as an  
273 effective parameter to constrain the light absorption enhancement of ambient BC-containing  
274 aerosols.

275 The new finding of our study is that the mixing state index can contribute to  
276 improvements in the accuracy of simulating the BC radiative effects. In the  
277 particle-resolved simulation of ambient aerosols, the particle-to-particle heterogeneity  
278 of BC-containing aerosols can be resolved by simply introduce the BC mixing state  
279 index  $\chi$ . Then the aerosol light absorption enhancement can be better constrained by  
280 MR and  $\chi$  and then the radiative effects of BC can be estimated. Therefore, our  
281 framework can be employed in the model by simply introduce a BC mixing state index  
282 for better estimating the BC radiative effects.

283  
284 **Data availability.** The data involved is available in the manuscript.

285 **Author contributions.** Gang Zhao wrote the manuscript. Chunsheng Zhao, Min Hu, Tianyi Tan,  
286 Song Guo, Zhijun Wu, Yishu Zhu and Gang Zhao discussed the results.

287 **Competing interests.** The authors declare that they have no conflict of interest.

288 **Acknowledgments.** This work is supported by the National Key R&D Program of China  
289 (2016YFC020000: Task 5) and the National Natural Science Foundation of China (41590872).

290  
291  
292  
293

294 Bohren, C. F., and Huffman, D. R.: Absorption and Scattering by a Sphere, in: Absorption and  
295 Scattering of Light by Small Particles, Wiley-VCH Verlag GmbH, 82-129, 2007.

296 Bond, T. C., and Bergstrom, R. W.: Light Absorption by Carbonaceous Particles: An Investigative  
297 Review, *Aerosol Sci. Technol.*, 40, 27-67, 10.1080/02786820500421521, 2006.

298 Bond, T. C., Doherty, S. J., Fahey, D. W., Forster, P. M., Berntsen, T., DeAngelo, B. J., Flanner, M.  
299 G., Ghan, S., Karcher, B., Koch, D., Kinne, S., Kondo, Y., Quinn, P. K., Sarofim, M. C., Schultz, M.  
300 G., Schulz, M., Venkataraman, C., Zhang, H., Zhang, S., Bellouin, N., Guttikunda, S. K., Hopke, P.  
301 K., Jacobson, M. Z., Kaiser, J. W., Klimont, Z., Lohmann, U., Schwarz, J. P., Shindell, D.,  
302 Storelvmo, T., Warren, S. G., and Zender, C. S.: Bounding the role of black carbon in the climate  
303 system: A scientific assessment, *J Geophys Res-Atmos*, 118, 5380-5552, 10.1002/jgrd.50171, 2013.

304 Bondy, A. L., Bonanno, D., Moffet, R. C., Wang, B., Laskin, A., and Ault, A. P.: The diverse  
305 chemical mixing state of aerosol particles in the southeastern United States, *Atmospheric Chemistry  
306 and Physics*, 18, 12595-12612, 10.5194/acp-18-12595-2018, 2018.

307 Cappa, C. D., Onasch, T. B., Massoli, P., Worsnop, D. R., Bates, T. S., Cross, E. S., Davidovits, P.,  
308 Hakala, J., Hayden, K. L., Jobson, B. T., Kolesar, K. R., Lack, D. A., Lerner, B. M., Li, S. M.,  
309 Mellon, D., Nuaaman, I., Olfert, J. S., Petaja, T., Quinn, P. K., Song, C., Subramanian, R., Williams,  
310 E. J., and Zaveri, R. A.: Radiative Absorption Enhancements Due to the Mixing State of  
311 Atmospheric Black Carbon, *Science*, 337, 1078-1081, 10.1126/science.1223447, 2012.

312 Cappa, C. D., Zhang, X., Russell, L. M., Collier, S., Lee, A. K. Y., Chen, C.-L., Betha, R., Chen, S.,  
313 Liu, J., Price, D. J., Sanchez, K. J., McMeeking, G. R., Williams, L. R., Onasch, T. B., Worsnop, D.  
314 R., Abbatt, J., and Zhang, Q.: Light Absorption by Ambient Black and Brown Carbon and its  
315 Dependence on Black Carbon Coating State for Two California, USA, Cities in Winter and Summer,  
316 *Journal of Geophysical Research: Atmospheres*, 124, 1550-1577, 10.1029/2018jd029501, 2019.

317 Ching, J., Fast, J., West, M., and Riemer, N.: Metrics to quantify the importance of mixing state for  
318 CCN activity, *Atmospheric Chemistry and Physics*, 17, 7445-7458, 10.5194/acp-17-7445-2017,  
319 2017.

320 Cui, X., Wang, X., Yang, L., Chen, B., Chen, J., Andersson, A., and Gustafsson, Ö.: Radiative  
321 absorption enhancement from coatings on black carbon aerosols, *Science of The Total Environment*,  
322 551-552, 51-56, doi.org/10.1016/j.scitotenv.2016.02.026, 2016.

323 Dickau, M., Olfert, J., Stettler, M. E. J., Boies, A., Momenimovahed, A., Thomson, K., Smallwood,  
324 G., and Johnson, M.: Methodology for quantifying the volatile mixing state of an aerosol, *Aerosol*  
325 *Sci. Technol.*, 50, 759-772, 10.1080/02786826.2016.1185509, 2016.

326 Fierce, L., Bond, T. C., Bauer, S. E., Mena, F., and Riemer, N.: Black carbon absorption at the global  
327 scale is affected by particle-scale diversity in composition, *Nature communications*, 7, 12361,  
328 10.1038/ncomms12361, 2016.

329 Fierce, L., Onasch, T. B., Cappa, C. D., Mazzoleni, C., China, S., Bhandari, J., Davidovits, P.,  
330 Fischer, D. A., Helgestad, T., Lambe, A. T., Sedlacek, A. J., 3rd, Smith, G. D., and Wolff, L.:  
331 Radiative absorption enhancements by black carbon controlled by particle-to-particle heterogeneity  
332 in composition, *Proceedings of the National Academy of Sciences of the United States of America*,  
333 117, 5196-5203, 10.1073/pnas.1919723117, 2020.

334 Jacobson, M. Z.: Short-term effects of controlling fossil-fuel soot, biofuel soot and gases, and  
335 methane on climate, Arctic ice, and air pollution health, *Journal of Geophysical Research:*  
336 *Atmospheres*, 115, n/a-n/a, 10.1029/2009JD013795, 2010.

337 Koch, D., Schulz, M., Kinne, S., and Mcnaughton, C.: Evaluation of black carbon estimations in  
338 global aerosol models, *Atmospheric Chemistry & Physics*, 9, 9001-9026, 2009.

339 Lan, Z.-J., Huang, X.-F., Yu, K.-Y., Sun, T.-L., Zeng, L.-W., and Hu, M.: Light absorption of black  
340 carbon aerosol and its enhancement by mixing state in an urban atmosphere in South China,  
341 *Atmospheric Environment*, 69, 118-123, 10.1016/j.atmosenv.2012.12.009, 2013.

342 Liu, D., Allan, J. D., Young, D. E., Coe, H., Beddows, D., Fleming, Z. L., Flynn, M. J., Gallagher, M.  
343 W., Harrison, R. M., Lee, J., Prevot, A. S. H., Taylor, J. W., Yin, J., Williams, P. I., and Zotter, P.:  
344 Size distribution, mixing state and source apportionment of black carbon aerosol in London during  
345 wintertime, *Atmospheric Chemistry and Physics*, 14, 10061-10084, 10.5194/acp-14-10061-2014,  
346 2014.

347 Liu, D., Whitehead, J., Alfarra, M. R., Reyes-Villegas, E., Spracklen, Dominick V., Reddington,  
348 Carly L., Kong, S., Williams, Paul I., Ting, Y.-C., Haslett, S., Taylor, Jonathan W., Flynn, Michael J.,  
349 Morgan, William T., McFiggans, G., Coe, H., and Allan, James D.: Black-carbon absorption  
350 enhancement in the atmosphere determined by particle mixing state, *Nature Geoscience*, 10, 184-188,  
351 10.1038/ngeo2901, 2017.

352 Liu, J., Li, X., Li, D., Xu, R., Gao, Y., Chen, S., Liu, Y., Zhao, G., Wang, H., Wang, H., Lou, S.,  
353 Chen, M., Hu, J., Lu, K., Wu, Z., Hu, M., Zeng, L., and Zhang, Y.: Observations of glyoxal and  
354 methylglyoxal in a suburban area of the Yangtze River Delta, China, *Atmospheric Environment*, 238,  
355 117727, 10.1016/j.atmosenv.2020.117727, 2020.

356 Liu, S., Aiken, A. C., Gorkowski, K., Dubey, M. K., Cappa, C. D., Williams, L. R., Herndon, S. C.,  
357 Massoli, P., Fortner, E. C., Chhabra, P. S., Brooks, W. A., Onasch, T. B., Jayne, J. T., Worsnop, D.  
358 R., China, S., Sharma, N., Mazzoleni, C., Xu, L., Ng, N. L., Liu, D., Allan, J. D., Lee, J. D., Fleming,  
359 Z. L., Mohr, C., Zotter, P., Szidat, S., and Prevot, A. S.: Enhanced light absorption by mixed source  
360 black and brown carbon particles in UK winter, *Nature communications*, 6, 8435,  
361 10.1038/ncomms9435, 2015.

362 Menon, S., Hansen, J., Nazarenko, L., and Luo, Y.: Climate effects of black carbon aerosols in China  
363 and India, *Science*, 297, 2250-2253, 10.1126/science.1075159, 2002.

364 Müller, T., Laborde, M., Kassell, G., and Wiedensohler, A.: Design and performance of a  
365 three-wavelength LED-based total scatter and backscatter integrating nephelometer, *Atmos. Meas.*  
366 *Tech.*, 4, 1291-1303, 10.5194/amt-4-1291-2011, 2011.

367 Nakayama, T., Ikeda, Y., Sawada, Y., Setoguchi, Y., Ogawa, S., Kawana, K., Mochida, M., Ikemori,  
368 F., Matsumoto, K., and Matsumi, Y.: Properties of light-absorbing aerosols in the Nagoya urban area,  
369 Japan, in August 2011 and January 2012: Contributions of brown carbon and lensing effect, *Journal*  
370 *of Geophysical Research: Atmospheres*, 119, 7211-7217, 10.1002/2014JD021744, 2014.

371 Peng, J., Hu, M., Guo, S., Du, Z., Zheng, J., Shang, D., Levy Zamora, M., Zeng, L., Shao, M., Wu,  
372 Y.-S., Zheng, J., Wang, Y., Glen, C. R., Collins, D. R., Molina, M. J., and Zhang, R.: Markedly  
373 enhanced absorption and direct radiative forcing of black carbon under polluted urban environments,

374 Proceedings of the National Academy of Sciences, 113, 4266-4271, 10.1073/pnas.1602310113,  
375 2016.

376 Peng, J., Hu, M., Guo, S., Du, Z., Shang, D., Zheng, J., Zheng, J., Zeng, L., Shao, M., Wu, Y.,  
377 Collins, D., and Zhang, R.: Ageing and hygroscopicity variation of black carbon particles in Beijing  
378 measured by a quasi-atmospheric aerosol evolution study (QUALITY) chamber, Atmospheric  
379 Chemistry and Physics, 17, 10333-10348, 10.5194/acp-17-10333-2017, 2017.

380 Riemer, N., and West, M.: Quantifying aerosol mixing state with entropy and diversity measures,  
381 Atmospheric Chemistry and Physics, 13, 11423-11439, 10.5194/acp-13-11423-2013, 2013.

382 Riemer, N., Ault, A. P., West, M., Craig, R. L., and Curtis, J. H.: Aerosol Mixing State:  
383 Measurements, Modeling, and Impacts, Reviews of Geophysics, 57, 187-249,  
384 10.1029/2018rg000615, 2019.

385 Saleh, R., Hennigan, C. J., McMeeking, G. R., Chuang, W. K., Robinson, E. S., Coe, H., Donahue, N.  
386 M., and Robinson, A. L.: Absorptivity of brown carbon in fresh and photo-chemically aged  
387 biomass-burning emissions, Atmos. Chem. Phys., 13, 7683-7693, 10.5194/acp-13-7683-2013, 2013.

388 Saleh, R., Robinson, E. S., Tkacik, D. S., Ahern, A. T., Liu, S., Aiken, A. C., Sullivan, R. C., Presto,  
389 A. A., Dubey, M. K., Yokelson, R. J., Donahue, N. M., and Robinson, A. L.: Brownness of organics  
390 in aerosols from biomass burning linked to their black carbon content, Nature Geoscience, 7, 647,  
391 10.1038/ngeo2220, 2014.

392 Wu, Y., Cheng, T., Liu, D., Allan, J. D., Zheng, L., and Chen, H.: Light Absorption Enhancement of  
393 Black Carbon Aerosol Constrained by Particle Morphology, Environ Sci Technol, 52, 6912-6919,  
394 10.1021/acs.est.8b00636, 2018.

395 Xie, C., Xu, W., Wang, J., Liu, D., Ge, X., Zhang, Q., Wang, Q., Du, W., Zhao, J., Zhou, W., Li, J.,  
396 Fu, P., Wang, Z., Worsnop, D., and Sun, Y.: Light absorption enhancement of black carbon in urban  
397 Beijing in summer, Atmospheric Environment, 10.1016/j.atmosenv.2019.06.041, 2019.

398 Xue, H., Khalizov, A. F., Wang, L., Zheng, J., and Zhang, R.: Effects of coating of dicarboxylic  
399 acids on the mass-mobility relationship of soot particles, Environmental Science & Technology, 43,  
400 2787-2792, 2009a.

401 Xue, H., Khalizov, A. F., Wang, L., Zheng, J., and Zhang, R.: Effects of dicarboxylic acid coating on  
402 the optical properties of soot, *Physical Chemistry Chemical Physics*, 11, 7869-7875,  
403 10.1039/B904129J, 2009b.

404 Ye, Q., Gu, P., Li, H. Z., Robinson, E. S., Lipsky, E., Kaltsonoudis, C., Lee, A. K. Y., Apte, J. S.,  
405 Robinson, A. L., Sullivan, R. C., Presto, A. A., and Donahue, N. M.: Spatial Variability of Sources  
406 and Mixing State of Atmospheric Particles in a Metropolitan Area, *Environ Sci Technol*, 52,  
407 6807-6815, 10.1021/acs.est.8b01011, 2018.

408 Yu, C., Liu, D., Broda, K., Joshi, R., Olfert, J., Sun, Y., Fu, P., Coe, H., and Allan, J. D.:  
409 Characterising mass-resolved mixing state of black carbon in Beijing using a  
410 morphology-independent measurement method, *Atmospheric Chemistry and Physics*, 20, 3645-3661,  
411 10.5194/acp-20-3645-2020, 2020.

412 Yuan, C., Zheng, J., Ma, Y., Jiang, Y., Li, Y., and Wang, Z.: Significant restructuring and light  
413 absorption enhancement of black carbon particles by ammonium nitrate coating, *Environ Pollut*, 262,  
414 114172, 10.1016/j.envpol.2020.114172, 2020.

415 Zhang, R., Khalizov, A. F., Pagels, J., Zhang, D., Xue, H., and McMurry, P. H.: Variability in  
416 morphology, hygroscopicity, and optical properties of soot aerosols during atmospheric processing,  
417 *Proceedings of the National Academy of Sciences of the United States of America*, 105,  
418 10291-10296, 10.1073/pnas.0804860105, 2008.

419 Zhang, X., Mao, M., Yin, Y., and Wang, B.: Absorption enhancement of aged black carbon aerosols  
420 affected by their microphysics: a numerical investigation, *Journal of Quantitative Spectroscopy and  
421 Radiative Transfer*, 202, 90-97, 10.1016/j.jqsrt.2017.07.025, 2017.

422 Zhao, G., Tan, T., Zhao, W., Guo, S., Tian, P., and Zhao, C.: A new parameterization scheme for the  
423 real part of the ambient urban aerosol refractive index, *Atmos. Chem. Phys.*, 19, 12875-12885,  
424 10.5194/acp-19-12875-2019, 2019a.

425 Zhao, G., Tao, J., Kuang, Y., Shen, C., Yu, Y., and Zhao, C.: Role of black carbon mass size  
426 distribution in the direct aerosol radiative forcing, *Atmos. Chem. Phys.*, 19, 13175-13188,  
427 10.5194/acp-19-13175-2019, 2019b.



428 Zhao, G., Zhao, W., and Zhao, C.: Method to measure the size-resolved real part of aerosol refractive  
429 index using differential mobility analyzer in tandem with single-particle soot photometer,  
430 Atmospheric Measurement Techniques, 12, 3541-3550, 10.5194/amt-12-3541-2019, 2019c.

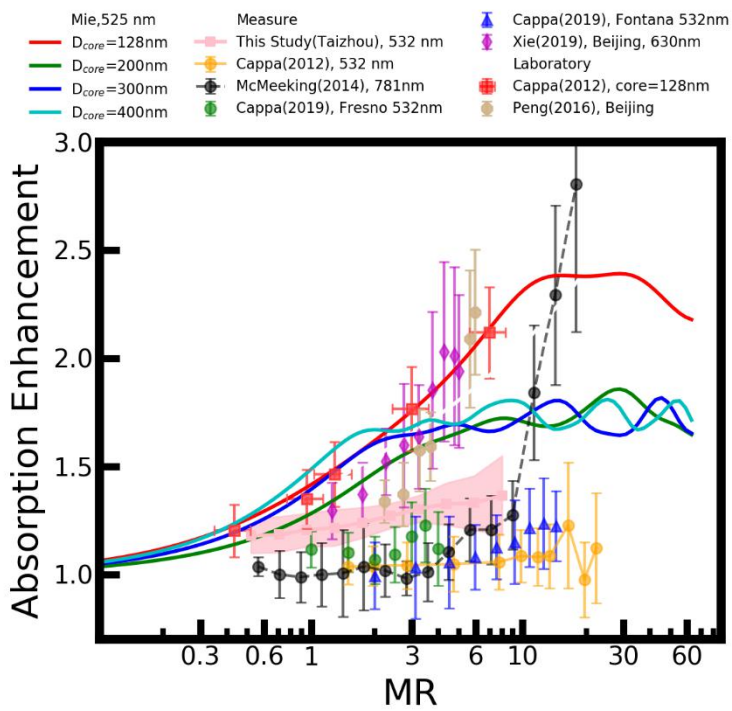
431 Zhao, G., Li, F., and Zhao, C.: Determination of the refractive index of ambient aerosols,  
432 Atmospheric Environment, 240, 117800, 10.1016/j.atmosenv.2020.117800, 2020a.

433 Zhao, G., Shen, C., and Zhao, C.: Technical note: Mismeasurement of the core-shell structure of  
434 black carbon-containing ambient aerosols by SP2 measurements, Atmospheric Environment, 243,  
435 117885, 10.1016/j.atmosenv.2020.117885, 2020b.

436 Zheng, Z., Curtis, J. H., Yao, Y., Gasparik, J. T., Anantharaj, V. G., Zhao, L., West, M., and Riemer,  
437 N.: Estimating Submicron Aerosol Mixing State at the Global Scale With Machine Learning and  
438 Earth System Modeling, Earth and Space Science, 8, 10.1029/2020ea001500, 2021.

439

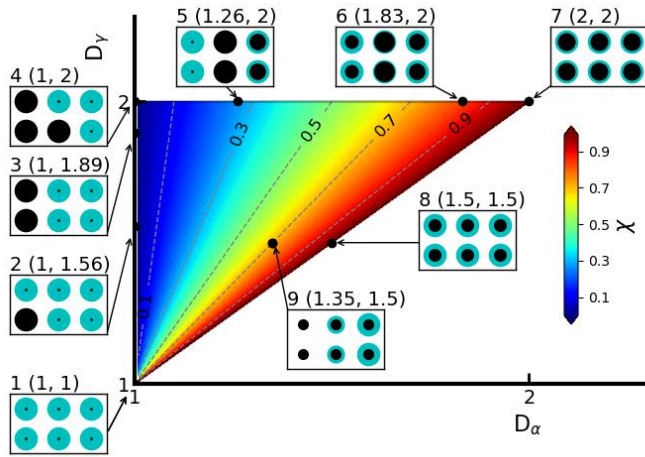
440



441

442 Figure 1. The measured  $E_{abs}$  of BC particles from different ambient measurements, including this  
 443 work (in pink), and lab studies.

444

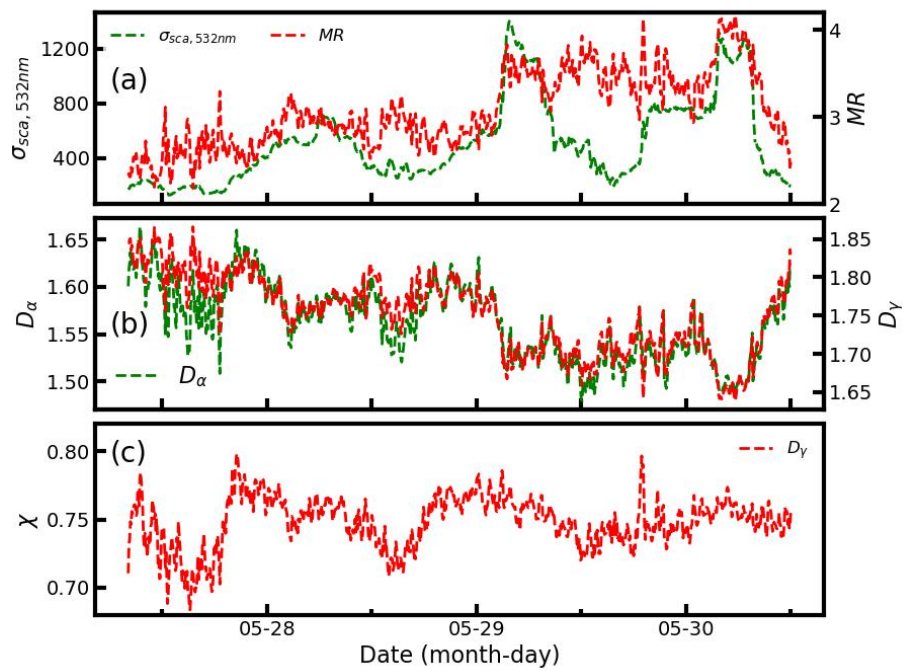


445

446 **Figure 2.** Mixing states diagram to illustrate the relationship between  $D_\alpha$ ,  $D_\gamma$ , and  $\chi$ . Each species

447 consists of six particles, and the colors of black and cyan represent the BC and non-BC components.

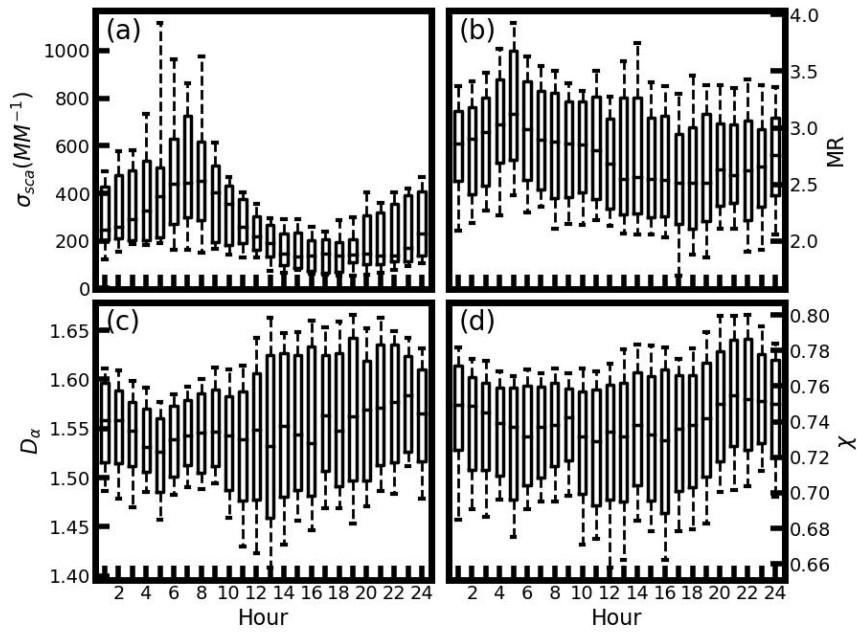
448



449

450 **Figure 3.** Measured time series of (a)  $\sigma_{sca}$  and MR, (b)  $D_\alpha$  and  $D_\gamma$ , and (c)  $\chi$ .

451

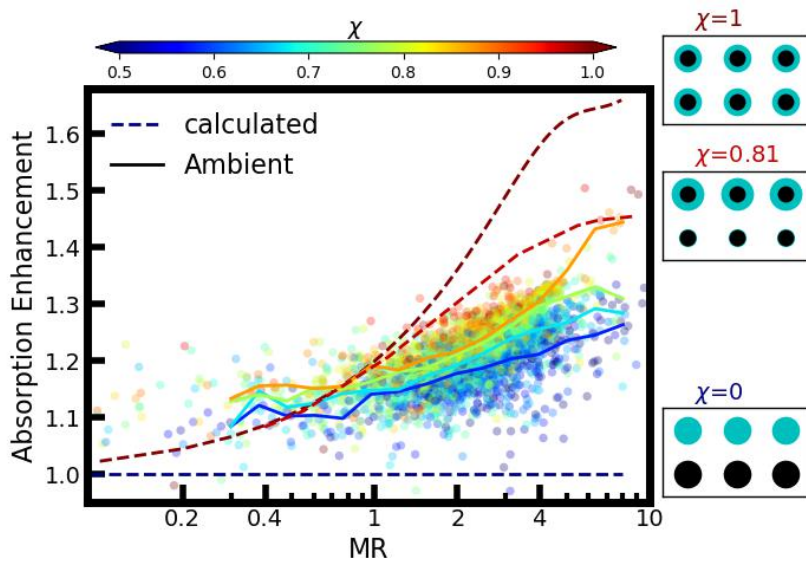


452

453 **Figure 4.** Daily variation of the measured (a)  $\sigma_{sca}$ , (b) MR, (c)  $D_\alpha$ , and (d)  $\chi$ .

454

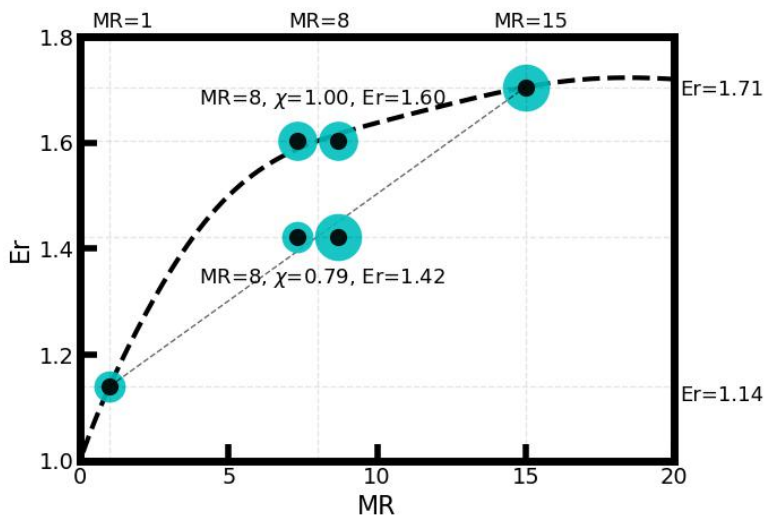
455



456

457 **Figure 5.** Relationship between the BC  $E_{abs}$  and the measured mass ratio of the BC-containing  
 458 aerosols coating material to BC under different  $\chi$  conditions. Four solid lines from bottom to up  
 459 corresponding to the measured ambient size-resolved BC mixing states data with  $\chi$  ranges of  
 460 0.575~0.625, 0.625~0.675, 0.675~0.725, and 0.725~0.775. The dotted line corresponds to the  $\chi$  of  
 461 0.0 (blue), 0.81 (light red), and 1.0 (dark red), respectively.

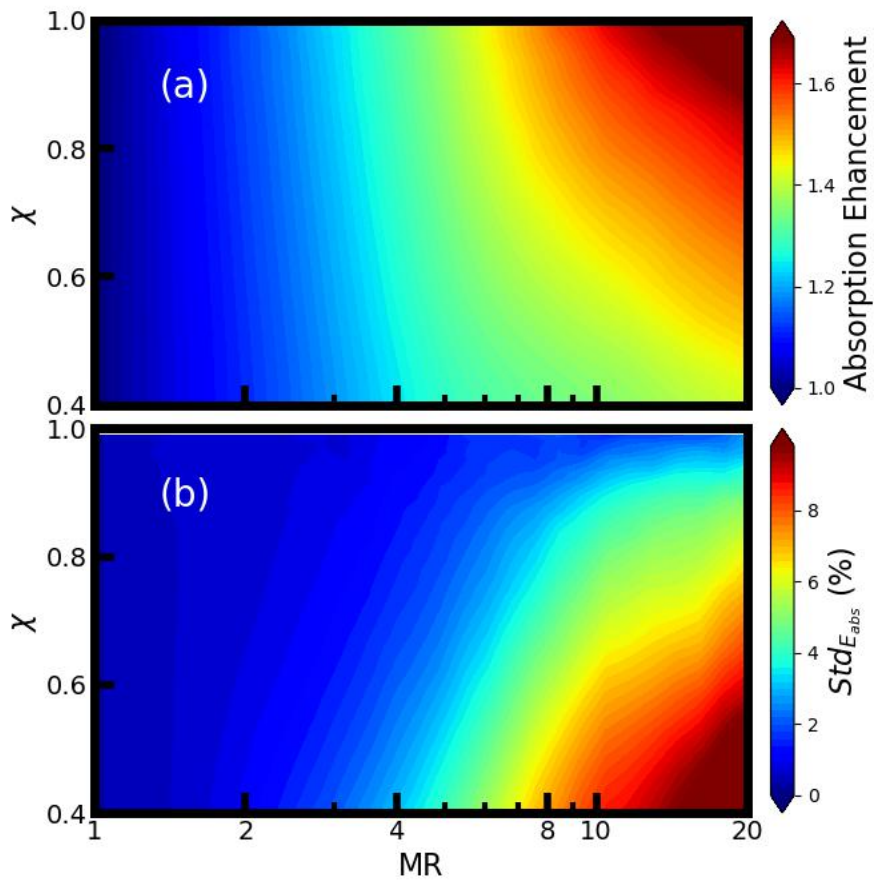
462



463

464 **Figure 6.** Schematic diagram that denotes the relationship between  $\chi$  and  $Er$ .

465



466

467 **Figure 7.** The calculated (a) mean  $E_{abs}$  values and (b) standard deviations of the  $E_{abs}$  values for  
 468 different MR and  $\chi$ .



ID	$(D_\alpha, D_\gamma)$	$\chi$	P1 <sup>*1</sup>	P2 <sup>*1</sup>	P3 <sup>*1</sup>	P4 <sup>*1</sup>	P5 <sup>*1</sup>	P6 <sup>*1</sup>	Tot <sup>*1</sup>
1	(1.00, 1.00)	-	(10 <sup>-9</sup> ,1)	(10 <sup>-9</sup> ,1)	(10 <sup>-9</sup> ,1)	(10 <sup>-9</sup> ,1)	(10 <sup>-9</sup> ,1)	(10 <sup>-9</sup> ,1)	(6·10 <sup>-9</sup> ,1)
2	(1.00,1.56)	0	(1,10 <sup>-9</sup> )	(10 <sup>-9</sup> , 1)	(10 <sup>-9</sup> , 1)	(10 <sup>-9</sup> , 1)	(10 <sup>-9</sup> , 1)	(10 <sup>-9</sup> , 1)	(1, 5)
3	(1.00, 1.89)	0	(1,10 <sup>-9</sup> )	(1,10 <sup>-9</sup> )	(10 <sup>-9</sup> , 1)	(10 <sup>-9</sup> , 1)	(10 <sup>-9</sup> , 1)	(10 <sup>-9</sup> , 1)	(2,4)
4	(1.00, 2.00)	0	(1,10 <sup>-9</sup> )	(1,10 <sup>-9</sup> )	(1,10 <sup>-9</sup> )	(10 <sup>-9</sup> , 1)	(10 <sup>-9</sup> , 1)	(10 <sup>-9</sup> , 1)	(3,3)
5	(1.26, 2.00)	0.26	(2,10 <sup>-9</sup> )	(2,10 <sup>-9</sup> )	(10 <sup>-9</sup> ,2)	(10 <sup>-9</sup> ,2)	(10 <sup>-9</sup> ,1)	(1,1)	(6, 6)
6	(1.83, 2.00)	0.83	(1,3)	(1,3)	(3,1)	(3,1)	(2,2)	(2,2)	(12,12)
7	(2.00, 2.00)	1.00	(1,1)	(1,1)	(1,1)	(1,1)	(1,1)	(1,1)	(6,6)
8	(1.5, 1.50)	1.00	(1,6.1)	(1,6.1)	(1,6.1)	(1,6.1)	(1,6.1)	(1,6.1)	(6, 36.6)
9	(1.35, 1.50)	0.70	(1,10 <sup>-9</sup> )	(1,10 <sup>-9</sup> )	(1,6.1)	(1,6.1)	(1,12.2)	(1,12.2)	(6, 36.6)

470 **Table 1.** Detail information of the BC particles shown in Fig.2

471 <sup>\*1</sup> Mass of the BC component of and non-BC component (arbitrary unit).